Carbohydrate Polymers 203 (2019) 26–34

Contents lists available at ScienceDirect

Carbohydrate Polymers

journal homepage: www.elsevier.com/locate/carbpol

# Antibacterial poly (3,4-ethylenedioxythiophene):poly(styrene-sulfonate)/agarose nanocomposite hydrogels with thermo-processability and self-healing

Youngsang Ko[a,1], Jeonghun Kim[b,1], Ho Young Jeong[a], Goomin Kwon[a], Dabum Kim[a], Minhee Ku[c], Jaemoon Yang[c], Yusuke Yamauchi[b], Hae-Yeong Kim[d], Chanhui Lee[a,*], Jungmok You[a,*]

[a] Department of Plant & Environmental New Resources, Kyung Hee University, 1732 Deogyeong-daero, Giheung-gu, Yongin-si, Gyeonggi-do 17104, South Korea
[b] School of Chemical Engineering & Australian Institute for Bioengineering and Nanotechnology (AIBN), The University of Queensland, QLD 4072, Australia
[c] Department of Radiology College of Medicine, Yonsei University, Seoul 03722, South Korea
[d] Institute of Life Sciences and Resources & Department of Food Science and Biotechnology, Kyung Hee University, 1732 Deogyeong-daero, Giheung-gu, Yongin-si, Gyeonggi-do 17104, South Korea

ARTICLE INFO

*Keywords:*
PEDOT:PSS
Agarose
Nanocomposite hydrogel
Self-healing
Photothermal
Antibacterial

ABSTRACT

Recently, Near-infrared (NIR)-induced photothermal killing of pathogenic bacteria has received considerable attention due to the increase in antibiotic resistant bacteria. In this paper, we report a simple aqueous solution-based strategy to construct an effective photothermal nanocomposite composed of poly(3,4-ethylenedioxythiophene):poly(styrene-sulfonate) (PEDOT:PSS) and agarose with thermo-processability, light triggered self-healing, and excellent antibacterial activity. Our experiments revealed that PEDOT:PSS/agarose was easily coated on both a 2D glass substrate and 3D cotton structure. Additionally, PEDOT:PSS/agarose can be designed into free-standing objects of diverse shape as well as restored through an NIR light-induced self-healing effect after damage. Taking advantage of strong NIR light absorption, PEDOT:PSS/agarose exhibited a sharp temperature increase of 24.5 °C during NIR exposure for 100 s. More importantly, we demonstrated that the temperature increase on PEDOT:PSS/agarose *via* photothermal conversion resulted in the rapid and effective killing of nearly 100% of the pathogenic bacteria within 2 min of NIR irradiation.

## 1. Introduction

It is becoming increasingly difficult to combat bacterial infection due to the emergence of multidrug resistant strains of bacteria, which leads to serious problems such as failure of medical devices and threats to global public health (Arciola, Campoccia, Speziale, Montanaro, & Costerton, 2012; Hall-Stoodley, Costerton, & Stoodley, 2004; Kim et al., 2015; Neoh, Li, Kang, Chiong, & Tambyah, 2017; Wei, Tang, Yu, & Chen, 2017). This has led to over 13 million deaths worldwide per year from infectious diseases (Song & Jang, 2014). A traditional antibiotics-based chemotherapy has several intrinsic limitations including solubility, overdosing, and systemic toxicity (Jeong, Sharker, In, & Park, 2015; Li et al., 2018; Zhang, Xia, Chen, Chen, & Wu, 2017). These current treatments are slow and destroy the bacteria chemically through lysis of pathogenic bacteria originating from interference with the normal metabolic process. Furthermore, antibiotic-resistant bacteria have been observed almost immediately after a new class of antibiotics are marketed (Molton, Tambyah, Ang, Ling, & Fisher, 2013; Zipperer et al., 2016). Thus, innovative antibacterial materials that are able to address microbial resistance as well as rapidly destroy pathogenic bacteria are in high demand.

Recently, near-infrared (NIR) laser-induced photothermal therapy has proven to be a versatile, powerful tool to combat cancer and bacterial infection (Chen, Fang, Tang, & Zheng, 2012; Chen, Tang, Tang, & Li, 2017; Chen et al., 2016; Wang et al., 2017; Wu, Deokar, Liao, Shih, & Ling, 2013; Yang et al., 2011; Zhang et al., 2018). NIR irradiation in the range of 700 – 1100 nm has a particularly large advantage in biological applications because it is deeply penetrable into tissues and is nearly harmless to living tissues, while ultraviolet (UV) is not (Boas, Elwell, Ferrari, & Taga, 2014; Ferrari & Quaresima, 2012; Manley, 2014). For selective and rapid hyper-thermal killing of pathogenic bacteria, the key component is a photothermal agent that can absorb NIR light (at

* Corresponding authors.
*E-mail addresses:* chan521@khu.ac.kr (C. Lee), jmyou@khu.ac.kr (J. You).
[1] These authors contributed equally to this work.

https://doi.org/10.1016/j.carbpol.2018.09.026
Received 10 July 2018; Received in revised form 6 September 2018; Accepted 13 September 2018
Available online 17 September 2018
0144-8617/ 

the range of 650–900 nm) and emit photothermal heat through a non-radiative mechanism. Therefore, a number of inorganic gold-based nanostructures have been extensively studied as potential photothermal killing agents (Chen et al., 2017; Jiang & Teng, 2017; Khantamat et al., 2015; Ran et al., 2017). In spite of their viability, the use of inorganic nanomaterials may be limited in future clinical applications since they are non-biodegradable, causing cytotoxic effects such as induction of oxidative stress (Hsiao et al., 2015; Jia et al., 2009; Lal, Clare, & Halas, 2008; Norman, Stone, Gole, Murphy, & Sabo-Attwood, 2008).

Hydrogels, which consist of physically or chemically cross-linked polymer chains, are soft materials with a high water content (Kim et al., 2016; Ko, Kim, Kim, Yamauchi et al., 2017; Thoniyot, Tan, Karim, Young, & Loh, 2015; Xing et al., 2016; You et al., 2015). A number of hydrogels are biocompatible and can be tailored to possess mechanical properties matching those of natural tissues and thus have been extensively utilized in a variety of applications including wound healing, surface coatings for implants, and antibacterial agents (Dhandayuthapani, Yoshida, Maekawa, & Kumar, 2011; Goldberg, Langer, & Jia, 2007; Spencer et al., 2017; Veiga & Schneider, 2013). Carefully designed photothermal agent-incorporated hydrogels can be promising antibacterial materials and coatings due to their ease of formation and the possibility for tailoring their physicochemical properties (size, surface chemistry, porosity, shape, stability, *etc.*) and photothermal performance.

In this study, the goal of this study is to present an antibacterial all-organic nanocomposite hydrogel composed of poly(3,4-ethylenedioxythiophene):poly(styrene-sulfonate) (PEDOT:PSS) and agarose with thermo-processability and self-healing ability. PEDOT:PSS, an aqueous-based conductive polymer nanoparticles with strong NIR absorbance, has recently emerged as a new NIR photothermal therapy (PTT) agent due to its water-dispersibility, high photothermal conversion efficiency, excellent photostability, and good biocompatibility (Jeong et al., 2015; Khan & Narula, 2016; Ko, Kim, Kim, & You, 2017; You et al., 2013). Agarose, one of the main polysaccharide components of agar, serves as the hydrogel backbone for antibacterial nanocomposite hydrogels. This physical agarose hydrogel can exhibit reversible sol-gel transition upon heating and cooling, originating from reversible cross-linking *via* hydrogen bonding, which enables to control size and shape and possess the self-healing performance (Hur et al., 2014; Park, Chae, Kim, & Hur, 2016; Wu et al., 2017). Because agarose gelation requires only a single component agarose without catalyst, agarose gel can be prepared more simply and rapidly than other gels by guar gum, celluloses, and other biopolymer materials. Based on these advantages of agarose, we have selected the agarose for preparation of functional hydrogel with photothermal properties. Recently, the fabrication of electroconductive hybrid microspheres has been reported by using PEDOT:PSS/agarose/polyvinyl alcohol(PVA)/$Fe_3O_4$ composite through microfluidic channel (Lee, Choi, Cho, & Yim, 2016). In contrast to previous study focusing on the electrical conductivity and magnetic property of hybrid microspheres, we describe here a simple aqueous solution-based strategy to construct spin-coatable, free-standing PEDOT:PSS/agarose composite hydrogel with excellent hemocompatibility and then demonstrated the potential bactericidal activities of PEDOT:PSS/agarose against pathogenic bacteria. In detail, by combining desirable properties of PEDOT:PSS and agarose hydrogel without any additives, we demonstrated that PEDOT:PSS/agarose all-organic nanocomposite hydrogel exhibited a rapid thermal response to NIR laser irradiation, resulting in complete bacterial death after 2 min irradiation, as well as possessing thermoplasticity and NIR light-assisted self-healing properties. We are not aware of studies investigating the use of PEDOT:PSS/agarose nanocomposite hydrogels for photothermal-based antibacterial activity. This conducting nanocomposite hydrogel with unique properties may find broad utility in future bioapplications, especially in photothermal therapy in pathogenic bacteria and cancer treatment, on-demand drug release systems responsive to electric field, light, and temperature, biomimetic devices such as artificial muscles, and organic bioelectronics devices.

## 2. Experimental section

### 2.1. Materials

Poly(3,4-ethylenedioxythiophene):poly(styrenesulfonate) (PEDOT:PSS) was purchased from Sigma-Aldrich and used without further purification. Agarose powder (MW: 120,000; sulfates content: < 0.10%) was purchased from Genomic Base. *tert*-Butyl alcohol and ethanol were purchased from Duksan Pure Chemicals Company Co., Ltd. (Korea). Phosphate buffered saline (PBS) was purchased from Life Technologies.

### 2.2. Preparation of agarose and PEDOT:PSS/agarose composite hydrogel

In general, 3 wt% agarose was mixed with DI water and the mixture was heated by a microwave oven to prepare a completely dissolved agarose precursor solution. To fabricate the PEDOT:PSS/agarose composite hydrogel, PEDOT:PSS (solid content: 1 wt%) solution was added to the agarose precursor solution with varying PEDOT:PSS concentrations (5, 10, 20, 40 v/v%). After the solution was thoroughly vortexed for two minutes, the mixture was poured onto a plastic petri dish and allowed to cool to room temperature. After gelation, the hydrogel was carefully peeled from the petri dish. The shape and size of the PEDOT:PSS/agarose composite hydrogel were easily adjusted with diverse molds. In addition, the PEDOT:PSS/agarose precursor solution was evenly coated on glass substrates and 3D cotton surfaces using spin-coating (500 rpm, 30 s) and dipping (2 min) methods, respectively.

### 2.3. Characterization of agarose and PEDOT:PSS/agarose composite hydrogel

The Fourier Transform infrared spectroscopy (FT-IR) measurements were recorded on FT-IR spectrophotometer (Spectrum One System, Perkin-Elmer) by dried samples. The morphologies of agarose and PEDOT:PSS/agarose composite aerogels were observed *via* field emission scanning electron microscopy (FE-SEM, Hitachi, model S-4200, Carl Zeiss, model Merlin). To prepare the SEM samples, the agarose and PEDOT:PSS/agarose composite hydrogel was converted to an aerogel *via* solvent exchange (water-ethanol-*t*-butyl alcohol) followed by freeze-drying (Kim et al., 2017). For this, 50 ml of water/ethanol and ethanol/*t*-butyl alcohol (75/25, 50/50, 25/75, 0/100) were exchanged at 30 min intervals, and 100% of the ethanol and *t*-butyl alcohol was used twice. The elemental analysis was performed using energy dispersive spectrometry (EDS).

The tests for swelling, porosity, and degradation properties of the prepared hydrogels were carried out by a gravimetric method (McBath & Shipp, 2010; Rennerfeldt, Renth, Talata, Gehrke, & Detamore, 2013; Sornkamnerd, Okajima, & Kaneko, 2017). The vacuum-dried agarose and PEDOT:PSS/agarose composite gels (diameter: 30 mm) were weighed and immersed in water for 3 days to calculate the swelling. For the porosity test, the freeze-dried samples were weighed and immersed in absolute ethanol for 1 day. The residual water or ethanol on the surface of swollen gel was removed before weighing. The swelling and porosity properties were calculated using Eqs. (1) and (2), respectively:

$$\text{Swelling} \quad (\%) = \frac{W_s - W_d}{W_d} \times 100 \tag{1}$$

$$\text{Porosity} \quad (\%) = \frac{W_s - W_d}{\rho V} \times 100 \tag{2}$$

where $W_s$ is the weight of swollen gel, $W_d$ is the weight of dry gel, ρ is the density of absolute ethanol and V is the volume of swollen gel. The degradation test of the hydrogels was performed by immersing in PBS buffer for 10 days. The degree of degradation was calculated using Eq.

(3):

$$\text{Degree of degradation } (\%) = \frac{W_t}{W_i} \times 100 \quad (3)$$

where $W_t$ is the weight of hydrogel after immersing time and $W_i$ is the initial weight of hydrogel.

The static contact angles of hydrogels were measured by contact angle/surface tension analyzer (FTA-200, First Ten Angstroms).

### 2.4. Measurements of photothermal performance

Ultraviolet − visible − near-infrared (UV–vis-NIR) absorption spectra were collected on a CARY 300 Bio (Varian) in the hydrogel state. The punched PEDOT:PSS/agarose gels (diameter: 12 mm) with different PEDOT:PSS concentrations were exposed to the laser beam (808 nm, power density: 2 W/cm$^2$, spot diameter: 14 mm) while the temperature was monitored with a digital thermometer (fluke 289 True RMS multimeter) with the probe (fluke-80bk-a). The probe was directly placed in contact with the edge of the top surface of each hydrogel. In addition, the probe was not directly exposed to the laser beam to prevent the effect of direct NIR irradiation on the temperature increase.

### 2.5. NIR induced self-healing of the PEDOT:PSS/agarose composite gel

To demonstrate the thermally induced self-healing of composite gel, the surface of PEDOT:PSS/agarose with 40 v/v% PEDOT: PSS was damaged by a scalpel. The laser was directed to the damaged surface for 1 min, resulting in partial melting. The gel was then left at room temperature. The microscopic images of the self-healed area were observed *via* optical microscopy (Nikon eclipse Ti-S).

### 2.6. Biocompatibility and hemocompatibility of the PEDOT:PSS/agarose composite gel

Biocompatibility test was performed by monitoring fibroblast cells incubated with composite gels for 4 days. The human fibroblast cell line CCD-986sk was obtained from the Korean Cell Line Bank (#KLCB21947, Republic of Korea) and cultured in IMDM (#12440-053, Gibco) medium supplemented with 10% fetal bovine serum (FBS) (Gibco) at 37 °C in a 5% $CO_2$. Cells were seeded into 12-microwell plates ($1 \times 10^4$ cells/well) and incubated for 24 h at 37 °C for stable adhesion. After 24 h of incubation, the PEDOT:PSS/agarose gels (20 v/v % and 40 v/v%) were added to the wells. These gels were cut to 1.0 mm diameter size by multi-purpose sampling tools for soft substrates (#69031-01, Miltex® Biopsy Punch with Plunger). For live/dead assay, cells were stained with ethidium homodimer-1 (EthD-1) and calcein AM (LIVE/DEAD® Viability/Cytotoxicity Kit, Thermo Fisher Scientific). Cells were monitored automatically at 30 min intervals for 4 days with Live Cell Imaging System (DMI6000B, Lecia Microsystems). The fluorescence microscopic images were captured using a DMI6000B and processed by the LAS X software.

Hemocompatibility of composite gels was examined by identifying hemolysis of red blood cells (RBCs). Blood sample from female Balb/c nude mouse was collected by 26 gauge 1 ml syringe into the sodium heparin-coated blood collection tubes (#367874, BD vacutainer®). The sample was kept at room temperature for 2 h and then centrifuged with 350 *g* for 15 min at 4 °C. After the removal of plasma and buffy coat layers, the gathered RBC cells (red layer) were washed 4 times with 1 ml of the physiological saline (0.9% w/v NaCl solution). The PEDOT:PSS/agarose gels (20 v/v% and 40 v/v%) were placed in a 12-well plate in triplicate. 1 ml of 30-fold diluted RBC suspension was added to each well. The positive control (RBC suspended in distilled water) and the negative control (RBC suspended in 0.9% NaCl solution) were used. The plate was incubated for 1 h at 37 °C without stirring, followed by centrifugation with 100 *g*, 5 min. 100 µl of the supernatant of all samples was transferred to a 96-well plate in triplicate. The optical density (OD) was measured at 540 nm by a microplate reader (Cytation 1, BioTek instruments). The hemolytic ratio was calculated as the following formula:

$$\text{Hemolysis ratio} = (OD_{sample} - OD_{negative\ control})/(OD_{positive\ control} - OD_{negative\ control}) \times 100\%$$

The RBC morphology was captured by DMI6000B (Leica Microsystems).

### 2.7. Bacteria culture

*Escherichia coli* (*E. coli*) DH5α strains were transformed with pENTR™-gus plasmid using a heat shock method. Transformant bacteria were grown in selection media Luria-Bertani (LB) agar (10 g/l tryptone, 10 g/l NaCl, and 5 g/l yeast extract) containing 50 µg/ml kanamycin overnight at 37 °C. A growth colony of bacteria was selected and cultured in LB media containing the same antibiotics overnight at 37 °C with shaking. In case of *Staphylococcus aureus* (*S. aureus*), bacteria were cultured in tryptic soy broth (TSB) overnight at 28 °C with shaking. Both cells were centrifuged at 4000 rpm for 5 min to harvest the bacterial pellet and were resuspended in sterile PBS solution. The concentration was adjusted to an $OD_{600}$ of 1.

### 2.8. Antibacterial activity after NIR exposure and a bacteria viability test

The photothermal antibacterial activities of the PEDOT:PSS/agarose composite hydrogel (40 v/v%) were examined against both bacteria (*E. coli* and *S. aureus*) by the following methods: 2 µl of each bacteria suspension ($OD_{600}$ = 1) was dropped onto the hydrogel (diameter: 6 mm) and softly spread with a loop. The bacteria on PEDOT:PSS/agarose gel was irradiated with the NIR laser (808 nm, power density: 2 W/cm$^2$, spot diameter: 14 mm) for 0 − 3 min and then collected by PBS buffer solution. After 10 min washing with shaking, 200 µl aliquots of each buffer were plated on the LB agar or tryptic soy agar (TSA) plate, spread gently, and incubated for 12 h at 37 °C or 28 °C. The control groups were treated by dropping the bacteria suspension onto the hydrogel without any NIR irradiation. Bactericidal activities were defined as a decrease in CFU/ml.

## 3. Results and discussion

In this study, we report a very simple procedure to fabricate an antibacterial all-organic nanocomposite hydrogel (PEDOT:PSS/agarose) with thermo-processability and self-healing ability. The use of PEDOT:PSS, which is a stable colloid in aqueous solution, as a photothermal agent allows us to conduct facile aqueous solution-based processing to construct PEDOT:PSS/agarose. This nanocomposite hydrogel was easily fabricated by simple mixing of the solutions of PEDOT:PSS and agarose in controlled ratios without sophisticated synthesis. As shown in Fig. 1A, PEDOT:PSS (1.0 wt%) was added to the agarose precursor solution at a temperature of 90 °C with different PEDOT:PSS concentrations (5, 10, 20, 40 v/v%) and then thoroughly vortexed for two minutes. Importantly, PEDOT:PSS could be easily mixed and the homogeneously well-mixed PEDOT:PSS/agarose solution was obtained due to the excellent affinity of two solutions. After cooling to room temperature, gelation of PEDOT:PSS/agarose was observed due to multiple hydrogen bonding crosslinks between PEDOT:PSS and/or agarose (Fig. 1B) (Agua et al., 2017; Armelin, Pérez-Madrigal, Alemán, & Díaz, 2016; Park et al., 2018). The hydrogen bonding between PEDOT:PSS and agarose in nanocomposite gels was clearly confirmed by FT-IR as shown in Fig. S1. The bands at ~3400 cm$^{-1}$ and ~1074 cm$^{-1}$ corresponding to −OH and –C–O–C– groups of agarose, respectively, were shifted towards lower wavenumber values in composite gel, indicating that there is hydrogen-bonding interaction between agarose and –$SO_3$H group on PSS of PEDOT:PSS (Hu et al., 2016;

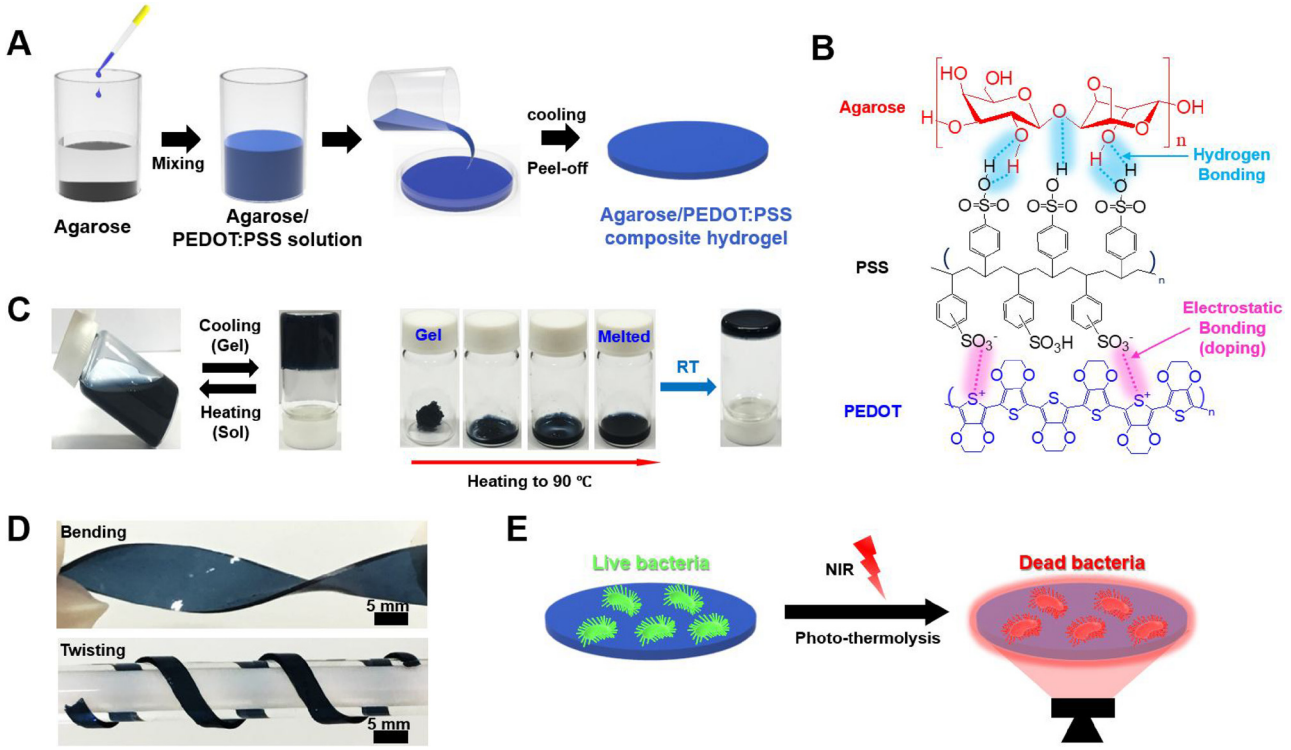


**Fig. 1.** Schematic illustration of (A) the fabrication procedure and (B) the interaction of PEDOT:PSS/agarose nanocomposite hydrogels (PEDOT:PSS concentrations: 5, 10, 20, and 40 v/v%). (C) Photographic presentation of the thermoplastic reversibility (sol-gel transition) of the PEDOT:PSS/agarose nanocomposite hydrogels with 40 v/v% PEDOT:PSS. (D) Photographs of PEDOT:PSS/agarose nanocomposite hydrogels with 40 v/v% PEDOT:PSS to show excellent bending and twisting properties. (E) Illustration of the photothermolysis of surface bacteria on the agarose/PEDOT:PSS composite hydrogel. The bacteria suspension was dropped onto the hydrogel and irradiated with the NIR laser (808 nm, power density: 2 W/cm$^2$).

Kadla & Kubo, 2003; Khan & Narula, 2016; Kuo & Chang, 2001).

During this physical gelation, the PEDOT:PSS/agarose composite became stable and homogeneous, resulting in a color change to dark blue. The color of the PEDOT:PSS/agarose became darker with an change of PEDOT:PSS concentration (Fig. 2A–C inset). It is important to note that there was no leakage of PEDOT:PSS from the composite hydrogel after immersion in water for a long time, indicating good stability of the PEDOT:PSS/agarose hydrogel. As expected in Fig. 1C, the PEDOT:PSS/agarose hydrogel exhibited reversible switching of the sol-gel transition upon thermal stimulus *via* multiple hydrogen bonds. Furthermore, PEDOT:PSS/agarose nanocomposite hydrogel shows excellent bending/twisting properties that are essential for various applications including integrated flexible biomedical devices (Fig. 1D). Finally, we demonstrated rapid and effective antibacterial activity by utilizing NIR laser-induced photothermal performance derived from PEDOT:PSS in the nanocomposite gel (discuss later, Fig. 1E).

The morphology of the pure agarose and PEDOT:PSS/agarose composite hydrogels was examined by scanning electron microscopy (SEM). As seen from the top surface SEM images (Fig. 2A–C), PEDOT:PSS/agarose nanocomposite hydrogel was rougher with a smaller curly layer structure than pure agarose. Importantly, the cross-sectional SEM images shown in Fig. 2D–F illustrate that PEDOT:PSS/agarose nanocomposite hydrogel with the highest PEDOT:PSS concentration (40 v/v%) was still present in the pore structure while PEDOT:PSS was uniformly dispersed in the gel matrix, demonstrating successful fabrication of the nanocomposite hydrogels.

We further investigated a set of EDS spectra of pure agarose and PEDOT:PSS/agarose to clearly confirm different components, in particular, the sulfur (S) element. According to the EDS results (Fig. 2G–I), the atomic percentage of S was 0.79 and 1.11% as the PEDOT:PSS concentration increased from 20 and 40 v/v%, respectively, while sulfate content was 0.35 at.% for pure agarose due to the purity of purchased agarose powder as a starting material. The increase of S content in composite gels resulted from the presence of S element on PEDOT and PSS.

We investigated the degree of swelling of pure agarose and composite hydrogels (agarose, 20 v/v%, and 40 v/v%) in water for 3 days as shown in Fig. S2A. Average mass swelling percentages for pure agarose, 20 v/v%, and 40 v/v% composite gel were observed to be 856, 706, and 315%, respectively. Analysis of hydrogel porosity (Fig. S2B) revealed that pure agarose, 20 v/v%, and 40 v/v% composite gels have showed 72, 69, and 60% porosity, respectively. These results indicated that the PEDOT:PSS has been incorporated well with the agarose, and then formed a stable hydrogel structure without breaking. As shown in Fig. S3, all hydrogels showed a small amount of weight loss after 10 days and only maximum 5% degradation was observed in 40 v/v% composite gel, indicating a good stability of the prepared composite hydrogels. The surface properties of agarose and composite gels were confirmed by contact angle. The contact angles of agarose and 20, 40 v/v% composite gels were found to be 60.14°, 47.54°, and 46.38°, respectively, probably due to the increase of hydrophilicity originated from a rich –$SO_3H$ groups on PSS.

The ability to construct an NIR-active photothermal coating as well as diverse shapes is very important for a variety of biomedical applications. Thus, we demonstrated the feasibility of fabricating PEDOT:PSS/agarose into stable coatings on various substrates and preprogrammed shapes. As shown in Fig. 3A, a thin PEDOT:PSS/agarose film was fabricated on a glass substrate by a spin coating method. Additionally, Fig. 3B illustrates that the PEDOT:PSS/agarose was evenly coated on the 3D cotton surface by simply immersing in the precursor PEDOT:PSS/agarose solution.

After immersion for a few minutes and cooling at room temperature for 10 min., a thin and uniform PEDOT:PSS/agarose coating was observed on the cotton fiber. This is a very efficient one-step method for

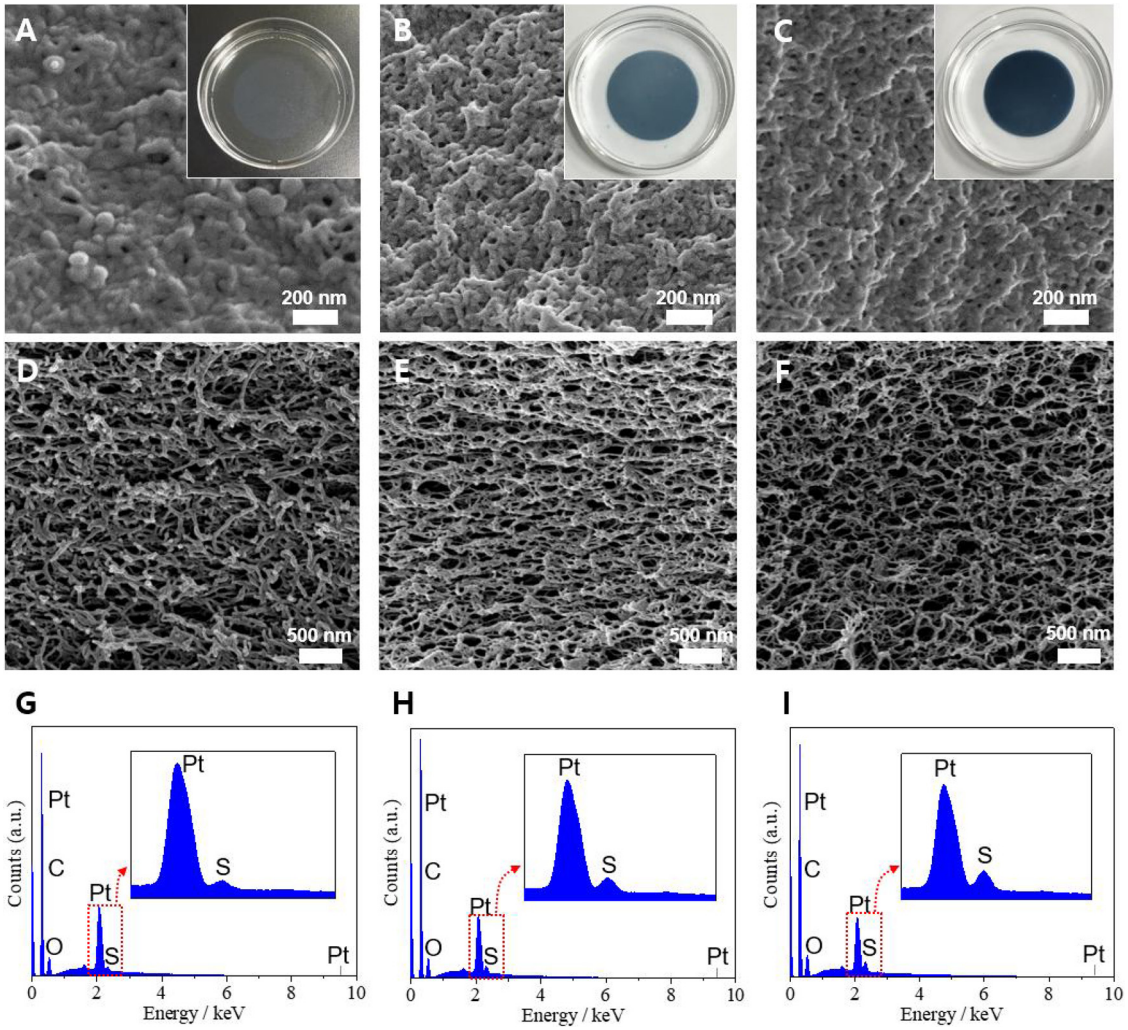


**Fig. 2.** FE-SEM images of (A–C) the surface and (D–F) cross-section (A, D: agarose; B, E: PEDOT:PSS/agarose of 20 v/v% PEDOT:PSS; C, F: PEDOT:PSS/agarose of 40 v/v% PEDOT:PSS). (Insets: Photographs of corresponding hydrogels). EDS spectra of (G) agarose, (H) PEDOT:PSS/agarose of 20 v/v% PEDOT:PSS, and (I) PEDOT:PSS/agarose of 40 v/v% PEDOT:PSS.

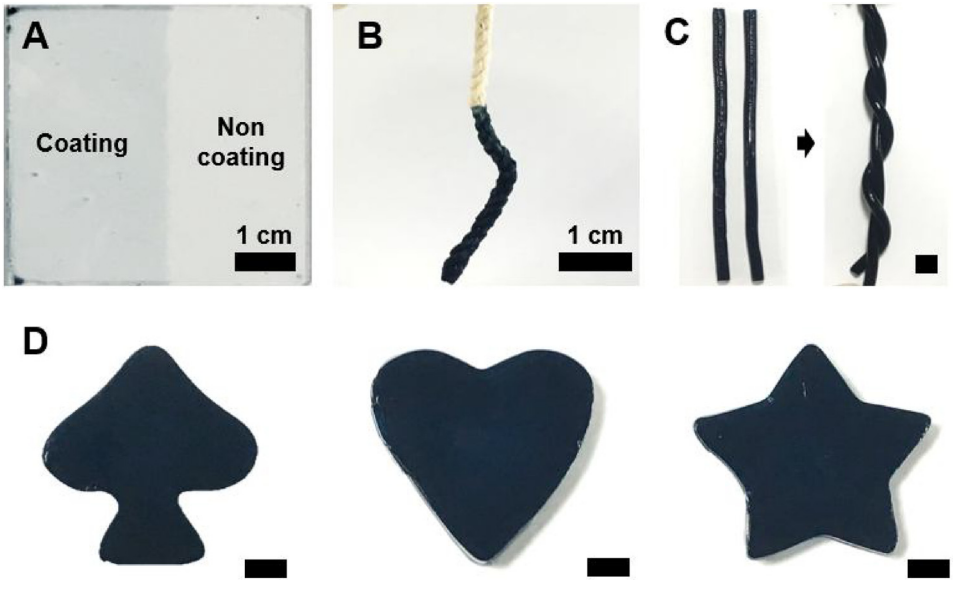


**Fig. 3.** Photographic images of PEDOT:PSS/agarose coated on (A) a smooth glass surface and (B) a 3D cotton surface. (A) The PEDOT:PSS/agarose was spin-coated on glass (500 rpm for 30 s). (B) The PEDOT:PSS/agarose was coated very thinly on the cotton surface by immersing in a PEDOT:PSS/agarose precursor solution for two minutes (middle) and cooling to room temperature. (C and D) Photographs of free-standing PEDOT:PSS/agarose with diverse shapes (coiled fiber, spade, heart, scale bar: 5 mm).

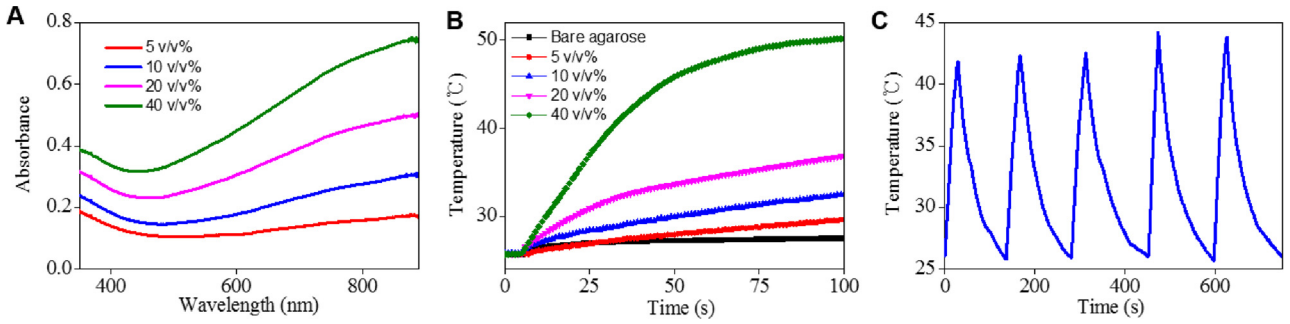


**Fig. 4.** (A) UV/vis spectra of PEDOT:PSS/agarose nanocomposite hydrogels of varying PEDOT:PSS concentrations (5, 10, 20, and 40 v/v%). (B) Photothermal heat generation of pure agarose and PEDOT:PSS/agarose of varying PEDOT:PSS concentrations (5, 10, 20, and 40 v/v%) under 808 nm laser irradiation with a power density of 2 W/cm$^2$. (C) Temperature change of PEDOT:PSS/agarose (40 v/v% PEDOT:PSS) over five cycles of NIR laser irradiation (808 nm, power density: 2 W/cm$^2$). The laser turned on for 30 s and then turned off when the temperature reached 26 °C.

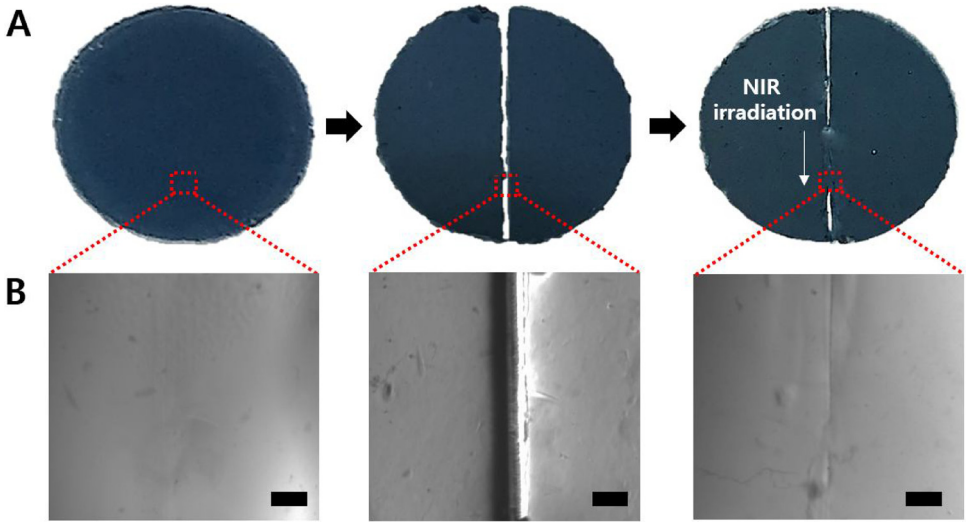


**Fig. 5.** (A) Photographic and (B) microscopic images of PEDOT:PSS/agarose of 40 v/v% PEDOT:PSS showing the NIR laser-triggered local self-healing property. NIR laser was applied to the damaged region of PEDOT:PSS/agarose for 1 min (NIR exposed area: 1 mm in diameter, scale bar: 200 μm).

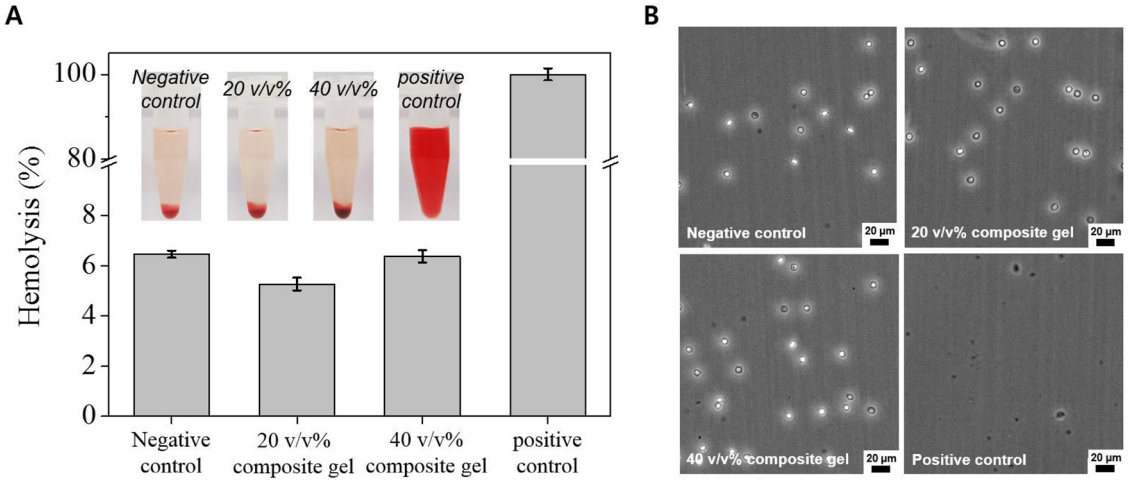


**Fig. 6.** (A) Hemolysis ratios and (B) optical microscopic images of RBCs after the hydrogels were incubated with RBCs for 1 h at 37 °C with shaking. (A inset) Images of RBCs after centrifugation of collected RBCs. The red solution indicates that the RBCs were destroyed and hemoglobin was released. (For interpretation of the references to colour in this figure legend, the reader is referred to the web version of this article.)

antibacterial coating. Interestingly, free-standing PEDOT:PSS/agarose of varying shape (fiber, spade, heart, star) was easily fabricated into a preprogrammed shape with a proper mold (Fig. 3C and D). PEDOT:PSS/agarose gel can be easily turned into a precursor solution by increasing temperature and then rapidly gelled to fix the shape *via* the reformation of hydrogen bonding by cooling to room temperature. Moreover, Fig. 3C reveals a stable coiled-coil structure with two PEDOT:PSS/agarose fibers (3 mm in diameter), demonstrating excellent flexibility of the PEDOT:PSS/agarose.

As shown in the absorption spectra presented in Fig. 4A, the NIR

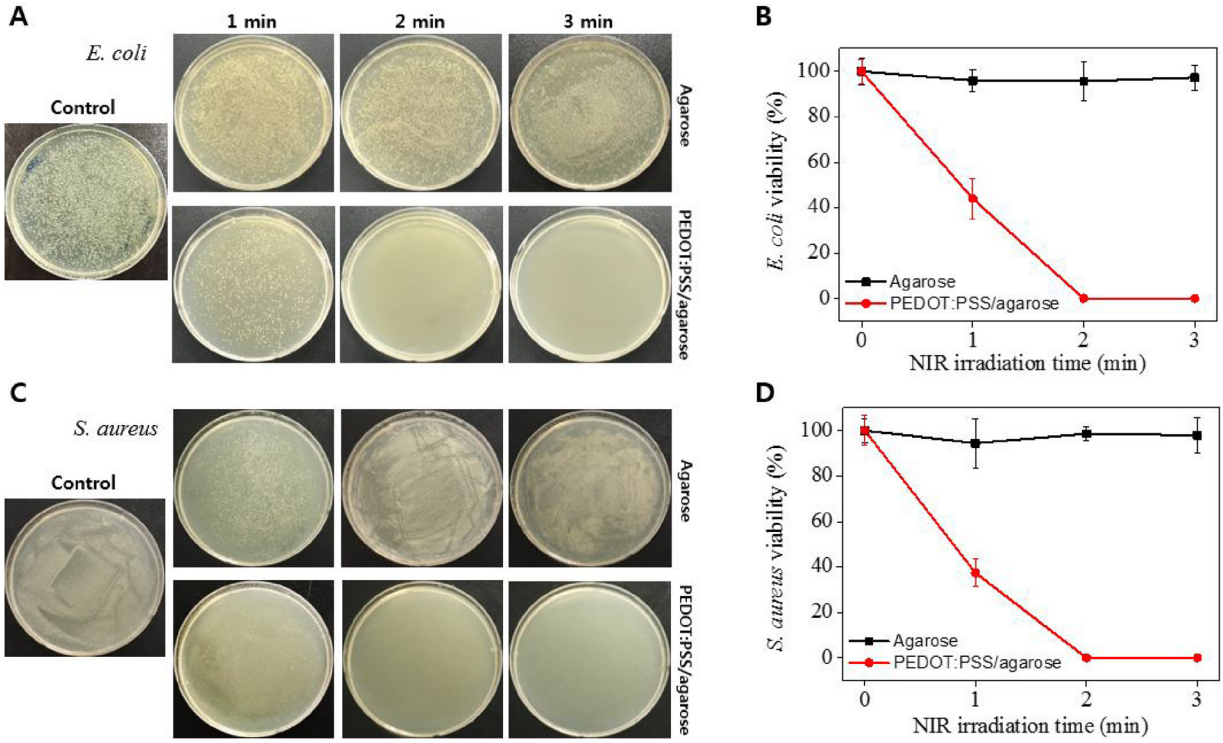


**Fig. 7.** Photographs of (A) *E. coli* and (C) *S. aureus* colonies regrown on LB agar or TSA plates by reseeding of collected PBS solution including bacteria from the agarose and 40 v/v% PEDOT:PSS/agarose hydrogels having 6 mm diameter after NIR irradiation (1–3 min). (B, D) The percentage of bacterial viability dependent on NIR exposure time for pure agarose and 40 v/v% PEDOT:PSS/agarose from A and C, respectively.

absorption of PEDOT:PSS/agarose was strong due to the formation of polaron and bipolaron states in PEDOT:PSS (You et al., 2013). NIR absorption of PEDOT:PSS/agarose gradually increased as the PEDOT:PSS concentration for PEDOT:PSS/agarose increased. The absorption of PEDOT:PSS/agarose with the highest PEDOT:PSS concentration (40 v/v%) at 808 nm was 4.4 times greater than that of PEDOT:PSS/agarose with the lowest PEDOT:PSS concentration (5 v/v%). We next analyzed the temperature change of PEDOT:PSS/agarose by NIR irradiation (808 nm, 2 W/cm$^2$, 100 s) to determine the NIR-induced photothermal effects (Fig. 4B). The pure agarose as a control showed a slightly elevated temperature around 2 °C, while PEDOT:PSS/agarose with different PEDOT:PSS concentrations of 5, 10, 20, and 40 v/v% exhibited a much greater temperature increase of 3.9, 6.7, 11.1, and 24.5 °C, respectively. The temperature increase of PEDOT:PSS/agarose by NIR irradiation was strongly dependent on the PEDOT:PSS amount, which is associated with the NIR absorption change of PEDOT:PSS/agarose shown in Fig. 4A. The highest PEDOT:PSS concentration (40 v/v%) showed a sharp temperature increase from 25.7 to 50.2 °C after NIR irradiation for 100 s, suggesting rapid and excellent photothermal conversion. Fig. 4C shows the temperate change of PEDOT:PSS/agarose with the highest PEDOT:PSS concentration over five cycles of NIR irradiation. The laser turned on for 30 s and then turned off when the temperature reached 26 °C. The temperature profile at each cycle was observed to be nearly the same, demonstrating that the PEDOT:PSS/agarose can endure repeated laser irradiation.

Thus, the PEDOT:PSS/agarose with the highest PEDOT:PSS concentration was chosen for further experiment related to NIR laser-induced self-healing property and antibacterial activity.

Fig. 5 represents the consecutive damage and healing processes of PEDOT:PSS/agarose to demonstrate the self-healing ability through NIR irradiation. After a cut of approximately 500 μm was made with a fine scalpel blade on the PEDOT:PSS/agarose surface, NIR light was intensively irradiated at the damaged sites for 1 min. The damaged site on PEDOT:PSS/agarose was partially melted by the local photothermal conversion. The PEDOT:PSS/agarose was clearly observed to be healed through the gelation process by cooling to room temperature. It is worth noting that the NIR-triggered temperature increase in PEDOT:PSS/agarose was localized only to the exposed region, which makes it uniquely suitable for diverse *in vivo* biomedical applications.

To investigate the biocompatibility of PEDOT:PSS/agarose composite gels, we carried out Live/Dead staining studies for samples obtained after the cultivation of fibroblasts for 4 days (Fig. S4). Similar to TCPS (positive control), most cells on PEDOT:PSS/agarose (20 v/v% and 40v/v%) appeared alive even though few dead cells on PEDOT:PSS/agarose were observed at 4 days. Hemolysis test was conducted to evaluate the hemocompatibility (blood compatibility) of PEDOT:PSS/agarose composite gels. As shown in Fig. 6A and B, the PEDOT:PSS/agarose (20 v/v% and 40 v/v%) didn't lead to a change in the apparent hemolysis. The hemolysis percentages caused by composite hydrogels were less than 6% when that of positive control (DI water) was set as 100%. These *in vitro* cell culture studies demonstrate that these composite hydrogels have good biocompatibility and excellent hemocompatibility.

We next analyzed the potential bactericidal activities of PEDOT:PSS/agarose (40 v/v% PEDOT:PSS) by different NIR exposure times (Fig. 7). There have been several reports demonstrating that increased temperature may cause irreversible cell injury due to destruction of metabolic signals, denaturation of protein, and rupture of cell walls (Li et al., 2016; Zhou et al., 2016). The suspensions of bacterial strains (*E. coli* and *S. aureus*) were first incubated on both pure agarose and PEDOT:PSS hydrogels, followed by NIR irradiation for 1, 2, and 3 min. *E. coli* and *S. aureus* were used to represent Gram-negative and Gram positive bacteria, respectively. Interestingly, both bacteria on pure agarose were nearly unaffected by NIR irradiation for 3 min., whereas the bactericidal activities of PEDOT:PSS/agarose was dependent on NIR irradiation time. Bacteria was not observed on PEDOT:PSS/agarose after 2 min of NIR irradiation (Fig. 7A, C). As shown in Fig. 7B and D, the *E. coli* and *S. aureus* viability significantly decreased to 44%

and 37% at 1 min of NIR irradiation, respectively. Moreover, both bacteria were completely killed after 2 min of NIR irradiation, suggesting excellent antibacterial activity of PEDOT:PSS/agarose comparing to previous reports. In comparison, graphene oxide based agent (Wu et al., 2013), gold nanoshell (AuNS)-modified Polydimethylsiloxane (PDMS) substrate (Khantamat et al., 2015), and Cu-nanoparticle incorporated in guar gum hydrogel (Chen et al., 2017) exhibited 99% bacteria killing efficiency at light intensities of 1.5 W/$cm^2$, 2.5 W/$cm^2$, 1.5 W/$cm^2$ after 10 min irradiation, respectively. In addition, iron oxide@PEDOT-based photothermal nanoparticles (Jeong et al., 2015) showed nearly 100% bacteria killing at light intensity of 2 W/$cm^2$ after 5 min. It is noteworthy that our optimized PEDOT:PSS/agarose hydrogel showed an effective killing of nearly 100% at light intensity of 2 W/$cm^2$ after 2 min. Importantly, the viability of both bacteria were nearly 100% on 40 v/v% PEDOT:PSS/agarose hydrogel without NIR irradiation, strongly indicating a good biocompatibility of the PEDOT:PSS/agarose nanocomposite.

## 4. Conclusions

We developed a novel photothermal nanocomposite based on PEDOT:PSS and agarose for antibacterial activity *via* a simple and rapid solution-based strategy. Due to the reversible sol-gel transition originating from reformable hydrogen bonds, in response to temperature change, the PEDOT:PSS/agarose exhibited thermo-plasticity allowing the design of diverse shapes as well as localized self-healing from external NIR exposure. The photothermal conversion of PEDOT:PSS/agarose by NIR irradiation plays an important role in antibacterial activity. The strong NIR absorption of PEDOT:PSS/agarose led to a sharp temperature increase within 100 s of NIR exposure. Furthermore, we demonstrated that *E. coli* and *S. aureus* bacteria were completely destroyed on PEDOT:PSS/agarose by 2 min of NIR irradiation, suggesting excellent antibacterial activity. Considering the simple production of a photothermal nanocomposite with flexibility, thermo-processability, localized self-healing, good biocompatibility, and effective bacterial killing, a PEDOT:PSS/agarose nanocomposite could enhance our abilities to engineer an antibacterial platform for practical applications. Future studies are in progress to develop a targeted chemo-phototherapy platform based on injectable PEDOT/PSS/agarose composite hydrogels which can realize NIR responsive controlled drug release as well as minimize damage to surrounding healthy tissue.

## Acknowledgements

This study was supported by a National Research Foundation of Korea (NRF) grant funded by the Korean government (MSIP) (No. 2017R1C1B2010867, 2018R1D1A1B07047874), a grant from Kyung Hee University in 2015 (KHU- 20152129), and a Cooperative Research Program for Agriculture Science and Technology Development (Project No. PJ01279701) Rural Development Administration, Republic of Korea.

## Appendix A. Supplementary data

Supplementary material related to this article can be found, in the online version, at doi:https://doi.org/10.1016/j.carbpol.2018.09.026.

## References

Agua, I. D., Mantione, D., Casado, N., Sanchez-Sanchez, A., Malliaras, G. G., & Mecerreyes, D. (2017). Conducting polymer iongels based on PEDOT and guar gum. *ACS Macro Letters, 6*(4), 473–478.

Arciola, C. R., Campoccia, D., Speziale, P., Montanaro, L., & Costerton, J. W. (2012). Biofilm formation in *Staphylococcus* implant infections. A review of molecular mechanisms and implications for biofilm-resistant materials. *Biomaterials, 33*(26), 5967–5982.

Armelin, E., Pérez-Madrigal, M. M., Alemán, C., & Díaz, D. D. (2016). Current status and challenges of biohydrogels for applications as supercapacitors and secondary batteries. *Journal of Materials Chemistry A, 4*, 8952–8968.

Boas, D. A., Elwell, C. E., Ferrari, M., & Taga, G. (2014). Twenty years of functional near-infrared spectroscopy: Introduction for the special issue. *NeuroImage, 85*, 1–5.

Chen, M., Fang, X., Tang, S., & Zheng, N. (2012). Polypyrrole nanoparticles for high-performance *in vivo* near-infrared photothermal cancer therapy. *Chemical Communications, 48*, 8934–8936.

Chen, R., Yang, F., Xue, Y., Wei, X., Song, L., & Liu, X. (2016). Polypyrrole confined in dendrimer-like silica nanoparticles for combined photothermal and chemotherapy of cancer. *RSC Advances, 6*, 38931–38942.

Chen, S., Tang, F., Tang, L., & Li, L. (2017). Synthesis of Cu-nanoparticle hydrogel with self-healing and photothermal properties. *ACS Applied Materials & Interfaces, 9*(24), 20895–20903.

Dhandayuthapani, B., Yoshida, Y., Maekawa, T., & Kumar, D. S. (2011). Polymeric scaffolds in tissue engineering application: A review. *International Journal of Polymer Science, 2011*, 290602.

Ferrari, M., & Quaresima, V. (2012). A brief review on the history of human functional near-infrared spectroscopy (fNIRS) development and fields of application. *NeuroImage, 63*, 921–935.

Goldberg, M., Langer, R., & Jia, X. (2007). Nanostructured materials for applications in drug delivery and tissue engineering. *Journal of Biomaterials Science Polymer Edition, 18*(3), 241–268.

Hall-Stoodley, L., Costerton, J. W., & Stoodley, P. (2004). Bacterial biofilms: From the natural environment to infectious diseases. *Nature Reviews Microbiology, 2*, 95–108.

Hsiao, C.-W., Chen, H.-L., Liao, Z.-X., Sureshbabu, R., Hsiao, H.-C., Lin, S.-J., et al. (2015). Effective photothermal killing of pathogenic bacteria by using spatially tunable colloidal gels with nano-localized heating sources. *Advanced Functional Materials, 25*(5), 721–728.

Hu, Z., Hong, P., Liao, M., Kong, S., Huang, N., Ou, C., et al. (2016). Preparation and characterization of chitosan—Agarose composite films. *Materials, 9*(10), 816.

Hur, J., Im, K., Kim, S. W., Kim, J., Chung, D.-Y., Kim, T.-H., et al. (2014). Polypyrrole/agarose-based electronically conductive and reversibly restorable hydrogel. *ACS Nano, 8*(10), 10066–10076.

Jeong, C. J., Sharker, S. M., In, I., & Park, S. Y. (2015). Iron oxide@PEDOT-based recyclable photothermal nanoparticles with poly(vinylpyrrolidone) sulfobetaines for rapid and effective antibacterial activity. *ACS Applied Materials & Interfaces, 7*(18), 9469–9478.

Jia, H. Y., Liu, Y., Zhang, X. J., Han, L., Du, L. B., Tian, Q., et al. (2009). Potential oxidative stress of gold nanoparticles by induced-NO releasing in serum. *Journal of the American Chemical Society, 131*(1), 40–41.

Jiang, S., & Teng, C. P. (2017). Fabrication of silver nanowires-loaded polydimethylsiloxane film with antimicrobial activities and cell compatibility. *Materials Science and Engineering C, 70*, 1011–1017.

Kadla, J. F., & Kubo, S. (2003). Miscibility and hydrogen bonding in blends of poly (ethylene oxide) and kraft lignin. *Macromolecules, 36*(20), 7803–7811.

Khan, S., & Narula, A. K. (2016). Bio-hybrid blended transparent and conductive films PEDOT:PSS:Chitosan exhibiting electro-active and antibacterial properties. *European Polymer Journal, 81*, 161–172.

Khantamat, O., Li, C.-H., Yu, F., Jamison, A. C., Shih, W.-C., Cai, C., et al. (2015). Gold nanoshell-decorated silicone surfaces for the near-infrared (NIR) photothermal destruction of the pathogenic bacterium *E. faecalis*. *ACS Applied Materials & Interfaces, 7*(7), 3981–3993.

Kim, D., Kim, J., Ko, Y., Shim, K., Kim, J. H., & You, J. (2016). A facile approach for constructing conductive polymer patterns for application in electrochromic devices and flexible microelectrodes. *ACS Applied Materials & Interfaces, 8*(48), 33175–33182.

Kim, H. J., Yang, Y. J., Oh, H. J., Kimura, S., Wada, M., & Kim, U.-J. (2017). Cellulose–silk fibroin hydrogels prepared in a lithium bromide aqueous solution. *Cellulose, 24*, 5079–5088.

Kim, S. H., Kang, E. B., Jeong, C. J., Sharker, S. M., In, I., & Park, S. Y. (2015). Light controllable surface coating for effective photothermal killing of bacteria. *ACS Applied Materials & Interfaces, 7*(28), 15600–15606.

Ko, Y., Kim, J., Kim, D., Yamauchi, Y., Kim, J. H., & You, J. (2017). A simple silver nanowire patterning method based on poly(ethylene glycol) photolithography and its application for soft electronics. *Scientific Reports, 7*, 2282.

Ko, Y., Kim, D., Kim, U.-J., & You, J. (2017). Vacuum-assisted bilayer PEDOT:PSS/cellulose nanofiber composite film for self-standing, flexible, conductive electrodes. *Carbohydrate Polymers, 173*, 383–391.

Kuo, S. W., & Chang, F. C. (2001). Miscibility and hydrogen bonding in blends of poly (vinylphenol-co-methyl methacrylate) with poly(ethylene oxide). *Macromolecules, 34*(12), 4089–4097.

Lal, S., Clare, S. E., & Halas, N. J. (2008). Nanoshell-enabled photothermal cancer therapy: Impending clinical impact. *Accounts of Chemical Research, 41*(12), 1842–1851.

Lee, S. W., Choi, J. S., Cho, K. Y., & Yim, J.-H. (2016). Facile fabrication of uniform-sized, magnetic, and electroconductive hybrid microspheres using a microfluidic droplet generator. *European Polymer Journal, 80*, 40–47.

Li, S., Dong, S., Xu, W., Tu, S., Yan, L., Zhao, C., et al. (2018). Antibacterial hydrogels. *Advanced Science, 5*(5), 1700527.

Li, S., Wang, X., Hu, R., Chen, H., Li, M., Wang, J., et al. (2016). Near-infrared (NIR)-absorbing conjugated polymer dots as highly effective photothermal materials for *in vivo* cancer therapy. *Chemistry of Materials, 28*(23), 8669–8675.

Manley, M. (2014). Near-infrared spectroscopy and hyperspectral imaging: Non-destructive analysis of biological materials. *Chemical Society Reviews, 43*, 8200–8214.

McBath, R. A., & Shipp, D. A. (2010). Swelling and degradation of hydrogels synthesized with degradable poly(β-amino ester) crosslinkers. *Polymer Chemistry, 1*, 860–865.

Molton, J. S., Tambyah, P. A., Ang, B. S., Ling, M. L., & Fisher, D. A. (2013). The global

spread of healthcare-associated multidrug-resistant bacteria: A perspective from Asia. *Clinical Infectious Diseases, 56*(9), 1310–1318.
Neoh, K. G., Li, M., Kang, E.-T., Chiong, E., & Tambyah, P. A. (2017). Surface modification strategies for combating catheter-related complications: Recent advances and challenges. *Journal of Materials Chemistry B, 5*, 2045–2067.
Norman, R. S., Stone, J. W., Gole, A., Murphy, C. J., & Sabo-Attwood, T. L. (2008). Targeted photothermal lysis of the pathogenic bacteria, *pseudomonas aeruginosa*, with gold nanorods. *Nano Letters, 8*(1), 302–306.
Park, J.-K., Kang, T.-G., Kim, B.-H., Lee, H.-J., Choi, H. H., & Yook, J.-G. (2018). Real-time humidity sensor based on microwave resonator coupled with PEDOT:PSS conducting polymer film. *Scientific Reports, 8*, 439.
Park, N., Chae, S. C., Kim, T., & Hur, J. (2016). Fabrication of self-healable and patternable polypyrrole/agarose hybrid hydrogels for smart bioelectrodes. *Journal of Nanoscience and Nanotechnology, 16*, 1400–1404.
Ran, X., Du, Y., Wang, Z., Wang, H., Pu, F., Ren, J., et al. (2017). Hyaluronic acid-templated Ag nanoparticles/graphene oxide composites for synergistic therapy of bacteria infection. *ACS Applied Materials & Interfaces, 9*(23), 19717–19724.
Rennerfeldt, D. A., Renth, A. N., Talata, Z., Gehrke, S. H., & Detamore, M. S. (2013). Tuning mechanical performance of poly(ethylene glycol) and agarose interpenetrating network hydrogels for cartilage tissue engineering. *Biomaterials, 34*, 8241–8257.
Song, J., & Jang, J. (2014). Antimicrobial polymer nanostructures: Synthetic route, mechanism of action and perspective. *Advances in Colloid and Interface Science, 203*, 37–50.
Sornkamnerd, S., Okajima, M. K., & Kaneko, T. (2017). Tough and porous hydrogels prepared by simple lyophilization of LC gels. *ACS Omega, 2*(8), 5304–5314.
Spencer, K. C., Sy, J. C., Ramadi, K. B., Graybiel, A. M., Langer, R., & Cima, M. J. (2017). Characterization of mechanically matched hydrogel coatings to improve the biocompatibility of neural implants. *Scientific Reports, 7*, 1952.
Thoniyot, P., Tan, M. J., Karim, A. A., Young, D. J., & Loh, X. J. (2015). Nanoparticle-hydrogel composites: Concept, design, and applications of these promising, multi--functional materials. *Advanced Science, 2*, 1400010.
Veiga, A. S., & Schneider, J. P. (2013). Antimicrobial hydrogels for the treatment of infection. *Biopolymers, 100*(6), 637–644.
Wang, X., Wang, C., Wang, X., Wang, Y., Zhang, Q., & Cheng, Y. (2017). A polydopamine nanoparticle-knotted poly(ethylene glycol) hydrogel for on-demand drug delivery and chemo-photothermal therapy. *Chemistry of Materials, 29*(3), 1370–1376.
Wei, T., Tang, Z., Yu, Q., & Chen, H. (2017). Smart antibacterial surfaces with switchable bacteria-killing and bacteria-releasing capabilities. *ACS Applied Materials & Interfaces, 9*(43), 37511–37523.
Wu, M.-C., Deokar, A. R., Liao, J.-H., Shih, P.-Y., & Ling, Y.-C. (2013). Graphene-based photothermal agent for rapid and effective killing of bacteria. *ACS Nano, 7*, 1281–1290.
Wu, Q., Wei, J., Xu, B., Liu, X., Wang, H., Wang, W., et al. (2017). A robust, highly stretchable supramolecular polymer conductive hydrogel with self-healability and thermo-processability. *Scientific Reports, 7*, 41566.
Xing, R., Liu, K., Jiao, T., Zhang, N., Ma, K., Zhang, R., et al. (2016). An injectable self-assembling collagen-gold hybrid hydrogel for combinatorial antitumor photothermal/photodynamic therapy. *Advanced Materials, 28*(19), 3669–3676.
Yang, J., Choi, J., Bang, D., Kim, E., Lim, E. K., Park, H., et al. (2011). Convertible organic nanoparticles for near-infrared photothermal ablation of cancer cells. *Angewandte Chemie International Edition, 50*(2), 441–444.
You, J., Haque, A., Shin, D.-S., Son, K. J., Siltanen, C., & Revzin, A. (2015). Bioactive photodegradable hydrogel for cultivation and retrieval of embryonic stem cells. *Advanced Functional Materials, 25*(29), 4650–4656.
You, J., Heo, J. S., Kim, J., Park, T., Kim, B., Kim, H.-S., et al. (2013). Noninvasive photodetachment of stem cells on tunable conductive polymer nano thin films: Selective harvesting and preserved differentiation capacity. *ACS Nano, 7*(5), 4119–4128.
Zhang, J., Feng, Y., Mi, J., Shen, Y., Tu, Z., & Liu, L. (2018). Photothermal lysis of pathogenic bacteria by platinum nanodots decorated gold nanorods under near infrared irradiation. *Journal of Hazardous Materials, 342*, 121–130.
Zhang, X., Xia, L.-Y., Chen, X., Chen, Z., & Wu, F.-G. (2017). Hydrogel-based phototherapy for fighting cancer and bacterial infection. *Science China Materials, 60*(6), 487–503.
Zhou, C., Wang, F., Chen, H., Li, M., Qiao, F., Liu, Z., et al. (2016). Selective antimicrobial activities and action mechanism of micelles self-assembled by cationic oligomeric surfactants. *ACS Applied Materials & Interfaces, 8*(6), 4242–4249.
Zipperer, A., Konnerth, M. C., Laux, C., Berscheid, A., Janek, D., Weidenmaier, C., et al. (2016). Human commensals producing a novel antibiotic impair pathogen colonization. *Nature, 535*, 511–516.